Intelligence 72 (2019) 67–75

Contents lists available at ScienceDirect

Intelligence

journal homepage: www.elsevier.com/locate/intell

Brain structural connectivity correlates with fluid intelligence in children: A DTI graph analysis

Gabriel Kocevar[a,1], Ilaria Suprano[a,1], Claudio Stamile[a], Salem Hannoun[b], Pierre Fourneret[c], Olivier Revol[c], Fanny Nusbaum[d], Dominique Sappey-Marinier[a,e,*]

[a] Univ Lyon, INSA-Lyon, Université Claude Bernard Lyon 1, UJM-Saint Etienne, CNRS, Inserm, CREATIS UMR 5220, U1206, F-69677, Lyon, France
[b] Nehme and Therese Tohme Multiple Sclerosis Center, Faculty of Medicine, American University of Beirut Medical Center, Beirut, Lebanon
[c] Hôpital Neurologique, Hospices Civils de Lyon, Service de Psychopathologie du développement de l'Enfant et de l'Adolescent, Bron, France
[d] Laboratoire Parcours Santé Systémique, (P2S, EA4129), Université de Lyon & Centre PSYRENE, France
[e] CERMEP - Imagerie du Vivant, Université de Lyon, Bron, France

ARTICLE INFO

Keywords:
MRI
Diffusion Tensor Imaging
Structural connectivity
Graph Theory
White Matter
Tractography
Intelligence Quotient

ABSTRACT

Purpose: The aim of this study is to better understand the neural substrate of intelligence in children, through the characterization of the brain's structural connectivity (graph measures), as well as the major white matter (WM) fibers microstructure.

Materials and methods: Fourty-three children (8 to 12 years) were include in this study. MRI acquisition included conventional and diffusion tensor imaging sequences. Children also underwent neuropsychological tests, providing the ten WISC-subtests. A factor analysis was performed to explore the inter-correlations of WISC-IV subtests and to extract intelligence domains as well as the general intelligence factor (g-score). Correlations between the intelligence domains and both graphs and diffusivity metrics were also explored.

Results: Global graph metrics revealed a strong relationship between high intelligence scores and brain network homogeneity (high density and low modularity), mainly in the temporal and parietal lobes. Furthermore, quantitative WM fiber-bundle analysis showed an increased axonal density in the major WM fiber-bundles that was associated to increased intelligence performances.

Conclusion: These findings demonstrated that intelligence neural substrate is based on a strong WM microstructure of the major intra- and inter- hemispheric fiber-bundles and a well-balanced network organization between local and global scales.

1. Introduction

Since the introduction of the first theory of general intelligence by Spearman(Barbey, 2018) and the first tests by Binet,(Basser et al., 2002) research on intelligence was mainly devoted to models conception,(Basser et al., 1994) and development of standardized scales to measure the intelligence quotient (IQ).(Basten et al., 2015) Nowadays, the neural substrate of intelligence can be investigated using the most advanced neuroimaging techniques, particularly magnetic resonance imaging (MRI). Indeed, this non-invasive technique provides both structural and functional information.(Beaulieu, 2002; Binet, 1905; Bullmore and Sporns, 2009) Based on the old idea that human intelligence depends on the brain size,(Carroll, 1993) MRI studies, conducted on large populations, showed small positive correlations between brain volume and intelligence.(Clayden et al., 2012; Colom et al., 2009) Gray matter (GM) and white matter (WM) volumes or densities also showed global and local correlations with IQ.(Colom et al., 2010; Desco et al., 2011; Desikan et al., 2006)

Functional MRI (fMRI) has also been used to investigate the relationship between intelligence and brain function, measured either by task-related or resting-state protocols.(Binet, 1905; Duncan, 2000; Dunst et al., 2014) Based on these studies, Jung and Haier have introduced the parieto-frontal integration theory (P-FIT) which pointed out a brain network composed of fourteen cerebral regions associated with elevated IQ.(Gogtay et al., 2004) More recently, a meta-analysis of Basten et al. including ten new studies, confirmed that cerebral activity is significantly correlated with intelligence in twelve of these regions.(Gray et al., 2003) Hilger et al. confirmed these observations by

* Corresponding author at: CERMEP – Imagerie du Vivant, 59 Boulevard Pinel, Bron 69677, France.
E-mail address: dominique.sappey-marinier@univ-lyon1.fr (D. Sappey-Marinier).
[1] These authors have contributed equally to this work.

https://doi.org/10.1016/j.intell.2018.12.003
Received 23 April 2018; Received in revised form 5 November 2018; Accepted 16 December 2018
Available online 28 December 2018
0160-2896/

showing that general intelligence depends on the topological organization of the fronto-parietal network (FPN) as well as the default mode network (DMN).(Hagmann et al., 2007) The results of these previous studies suggest a possible specific organization of the brain network topology, related to intelligence.(Haier et al., 2004) Indeed, authors suggested, that intelligence could depend "on the dynamic reorganization of brain networks, modifying their topology and community structure in the service of system-wide flexibility and adaptation".

Diffusion tensor imaging (DTI) also constitutes a very sensitive imaging tool for the characterization of WM microstructural organization and the identification of neural pathways.(Harris and Galton, 1870; Hilger et al., 2017; Jenkinson et al., 2012) Indeed, WM fiber organization and integrity in brain tissue can be measured through the estimation of diffusivity metrics such as the fractional anisotropy (FA), and the axial (AD) and radial (RD) diffusivities, estimating the amount of diffusion along and perpendicular to the main fiber direction. During the last decade, the high sensitivity of DTI to WM changes identified an association between WM microstructure and IQ from childhood to adulthood. Initially, Schmithorst et al. reported a positive association between IQ and FA in numerous cerebral regions of children.(Desco et al., 2011) More recently, a positive correlation between FA values and intelligence scores, was observed in several large WM fiber-bundles, namely the splenium of the corpus callosum, the left inferior longitudinal, and the arcuate fasciculi.(Jones et al., 2013) Muetzel et al. also reported a positive association between FA and both IQ and visuospatial abilities in children, mainly in the right uncinate fasciculus. (Jung and Haier, 2007) In a study of 168 subjects, aged between eight and 30 years, both verbal and performance abilities were positively associated to FA, particularly in the left hemisphere, independently of age and sex.(Karama et al., 2011) During adolescence, Navas-Sanchez et al. confirmed the correlation between IQ and FA, mainly in the corpus callosum,(Kim et al., 2016) while Dunst et al. showed that adults' WM microstructure differs between individuals as a function of intelligence and gender.(Kocevar et al., 2016) Along with the FA, AD may also be well correlated with IQ. Indeed, Nusbaum et al. showed increased AD in children with high IQ compared to standard IQ. This study also showed, that diffusivity measures could discriminate two groups of high IQ children profiles, namely homogeneous and heterogeneous.(Lee et al., 2006)

Based on a geometrical graph representation, a simple description of structural brain connectivity was recently proposed.(Li et al., 2009) Indeed, connections between GM regions, represented as graph nodes, can be derived from DTI tractography. Using such formalism, the brain could be considered as a small-world network, whose organization can be explored at both local and global scales using graph theory.(Lou et al., 2004) The relationship between graphs structural connectivity and IQ was first evaluated in adults by Li et al., showing higher global efficiency (E_g) and shorter characteristic path length (L) in subjects with higher IQ scores.(McDaniel, 2005) A recent study, performed in a population of 99 children (six to eleven years old), showed that E_g was correlated to the perceptual reasoning index (PRI) and its subtests. (Mori and Zhang, 2006) Furthermore, this study highlighted several associations between local network organization and intelligence. Indeed, PRI sub-scores were positively correlated to local efficiency in the pre- and post-central gyrus, the precuneus, the superior and inferior frontal gyri, and in the inferior temporal cortex. However, this unique study in children was limited to the analysis of only PRI and its subtests.

In the present study, we propose to explore the neural substrate of intelligence in a cohort of children. We tested the hypothesis that intelligence is associated with a better structural connectivity and a specific network organization at different anatomical levels: whole brain, intra- and inter-hemispheres, and lobes. The relationship between diffusion metrics and the major intelligence domains, based on the Wechsler intelligence scale for children (WISC-IV) subtests intercorrelations, was first assessed in the main WM fiber-bundles. Second, the brain structural networks properties were investigated using a graph theory approach at both global and local scales.

2. Material and methods

2.1. Participants

This prospective MRI study (conceived by F.N.) included 43 children (11 girls and 32 boys, age (mean ± SD): 9.82 ± 1.06 years). Subjects were recruited from the private psychological center (PSYRENE) and the children's psychiatry unit of Lyon's Neurological Hospital, both specialized in high IQ children evaluation and follow-up, as well as through advertisement in medical practices and public institutions. All children with any neurological diseases, medical psychiatric comorbidities, learning disabilities, psychotropic treatments, or contra-indications for MRI were excluded. Prior to enrollment, children received a medical examination and were fully informed along with their parents of the study details. Ethical committee approval ("CPP Sud-Est IV") and written informed consent from the children and their parents were obtained.

2.2. Intelligence scores

All children underwent comprehensive neuropsychological testing using the WISC-IV which provided a reliable estimation of the full-scale IQ (FSIQ) based on ten subtests, namely the vocabular, comprehension, and similarities subtests (estimating the verbal comprehension abilities), the picture concept, matrix reasoning, and block design (reflecting the perceptual reasoning abilities), the letter-number sequencing and digit span subtests (estimating the working memory), and the coding and symbol search subtests (estimating the processing speed).

2.3. MRI acquisition and processing

MRI examinations were performed without any sedation or contrast agent at the MRI department of the CERMEP-Imagerie du Vivant, on a 1.5 T Siemens Sonata system (Erlangen, Germany) with an 8-channels head-coil and 40mT/m gradients. The MRI protocol included a 3D T1-weighted magnetization prepared rapid gradient echo (MPRAGE) sequence (time of repetition / time of echo / time for inversion [TR/TE/TI] = 1970/3.93/1100 *ms*; flip angle = 15°; matrix size = 256 × 256; field of view = 256 × 256 *mm*; slice thickness = 1 *mm*; voxel size = 1x1x1 *mm*; acquisition time = 8 min). DTI protocol was based on a 2D multi-slice spin-echo echo-planar imaging (EPI) sequence (TR/TE = 6900/86 *ms*, resolution 2.5 × 2.5 × 2.5 *mm*, FOV = 240 × 240 *mm*, acquisition time = 7 *min*). Fifty-one contiguous axial slices were acquired in the anterior commissure - posterior commissure (AC-PC) plane. Twenty-four diffusion gradient directions (b = 1000 s/mm^2) were applied. The b0 image was acquired four times to increase signal to noise ratio while other directions were acquired twice.

Diffusion data were corrected for subjects' motion and Eddy currents using the FMRIB Software Library (FSL).(Muetzel et al., 2015) Non-brain voxels were removed using FSL-BET. Transformation matrices generated during the Eddy current correction were also used to compute the Root Mean Square deviation. As a result, we obtained a mean patient displacement value of 1.26 ± 0.52 *mm* (mean ± SD), which is half of a voxel size (2.5 *mm*). For each subject, the tensor model was then fitted on diffusion data using FSL-FDT and four diffusion maps (FA, AD, RD, and mean diffusivity (MD)) were extracted.(Navaschez et al., 2014)

Both T1-weighted and DTI data were visually inspected (GK, SH & D.S-M) in order to detect artifacts arising from subject motion or scanner malfunction and confirm the lack of visually detectable abnormalities.

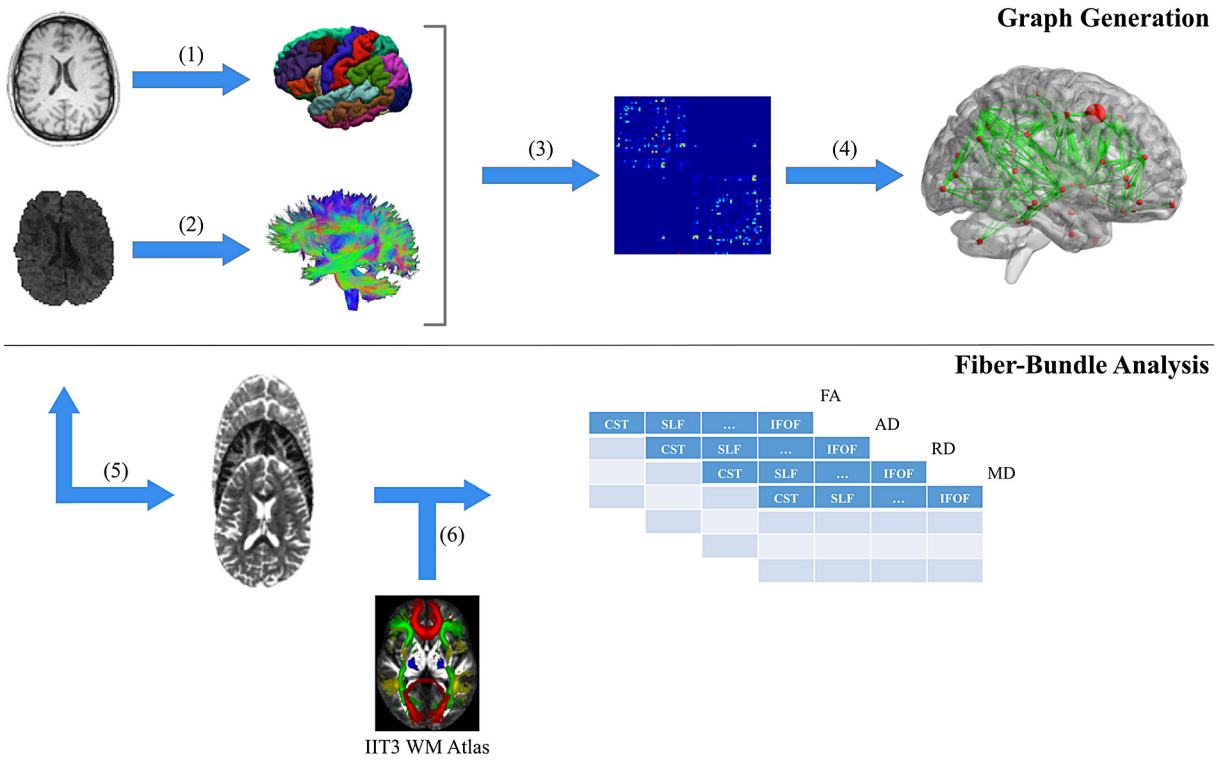

Fig. 1. Overview of the pipeline used for data processing. On top, the pipeline for graph generation: graph nodes are generated through anatomical parcellation on T1 image (Spearman, 1904) and probabilistic anatomically constrained streamline tractography is generated from diffusion images (Binet, 1905). Then, the numbers of streamlines connecting each pair of nodes are used to define edges in the weighted graph and generate the connectivity matrices. (Carroll, 1993) Finally, a proportional threshold ($\tau = 0.25$) was applied to remove the weakest connections before generating adjacency matrices (Wechsler, 2004). On bottom, the pipeline for fiber-bundles extraction. Computation of FA, MD, AD, and RD (Duncan, 2000) from diffusion images. Registration of the atlas on the subject space (Gray et al., 2003) and extraction of the mean value inside WM masks.

2.4. Fiber-bundle analysis

Large WM fiber-bundles were defined using the Illinois Institute of Technology (IIT) atlas, which included the forceps major (Fmajor), the forceps minor (Fminor), the superior and inferior longitudinal fasciculus (SLF and ILF respectively), the inferior fronto-occipital fasciculus (IFOF), the uncinate fasciculus (Unc), the cingulum (Cing), and the cortico-spinal tract (CST).(Nusbaum et al., 2017) The IIT atlas FA map was co-registered to each subject's FA image using a non-rigid transformation performed using NiftyReg (Oshio et al., 2010) The resulting deformation field was then applied to co-register the IIT atlas large WM fiber-bundles to each patient's space. Since fiber-bundles masks contained the probability of each voxel to belong to a specific fiber-bundle, a threshold was used to discard all voxels having a probability lower than 35%. The resulting masks were then binarized. Finally, the mean value of FA, MD, AD, and RD, were extracted from each subject's fiber-bundles. This pipeline for fiber-bundles analysis is illustrated in Fig. 1.

2.5. Graphs analysis

The previously generated deformation field was used to transform the Desikan cortical and subcortical GM parcellation to each subject space, to define the 84 nodes of the structural brain networks.(Ourselin et al., 2001)

Whole brain tractography was performed for every subject using MRtrix software.(Privado et al., 2017) First, the main diffusion directions were estimated in each voxel using diffusion orientation distribution function (dODF). The maximum spherical harmonics order $h = 4$ was selected to match with the acquisition protocol. Then, based on the four-tissue-class classification (WM, cortical GM, sub-cortical GM and cerebro-spinal fluid (CSF)) of the IIT atlas and dODF, anatomically constrained probabilistic streamline tractography was performed to generate 1′000’000 streamlines. Finally, adjacency matrices were generated for each subject by summing the number of streamlines connecting each pair of nodes. In order to remove the weakest connections generated by tractography, a proportional threshold (τ) must be applied to obtain binary connectivity matrices. As this threshold strongly affects the network topology and density, it has to be carefully chosen.(Reuter et al., 2012; Rubinov and Sporns, 2010) Two methods are commonly used in brain network studies, namely absolute and proportional thresholding. In this work, proportional threshold $\tau = 0.25$ was selected according to the method described elsewhere.(Schmithorst et al., 2005) The pipeline for graph generation is illustrated in Fig. 1.

Brain structural connectivity was analyzed globally as well as locally by dividing the connectivity matrices in different sub-graphs: the left and right hemispheres, and the inter-hemisphere connections graph. The connectivity matrices were also divided into subnetworks of lobes (frontal, occipital, parietal and temporal), and sub-cortical nuclei. Details of the cortical regions composing each lobe and a schematic representation of this subdivision on the connectivity matrix is shown in Fig. 2.

The topological properties of brain networks were analyzed using global and nodal metrics from graph theory.(Shaw et al., 2006) Six global graph metrics were estimated to analyze the networks properties. First, the graph density ($\boldsymbol{D}$) is measured as the ratio between the numbers of effective connections in the graph ($\boldsymbol{l}$) to the number of possible connections. Second, the integration property of the graph was evaluated using the following two metrics: the characteristic path length ($\boldsymbol{L}$), which is the mean of the shortest paths in the graph, and the global efficiency ($\boldsymbol{E_g}$), which is the mean of the inverse of the distance matrix of the graph. Third, the segregation property of the graph was

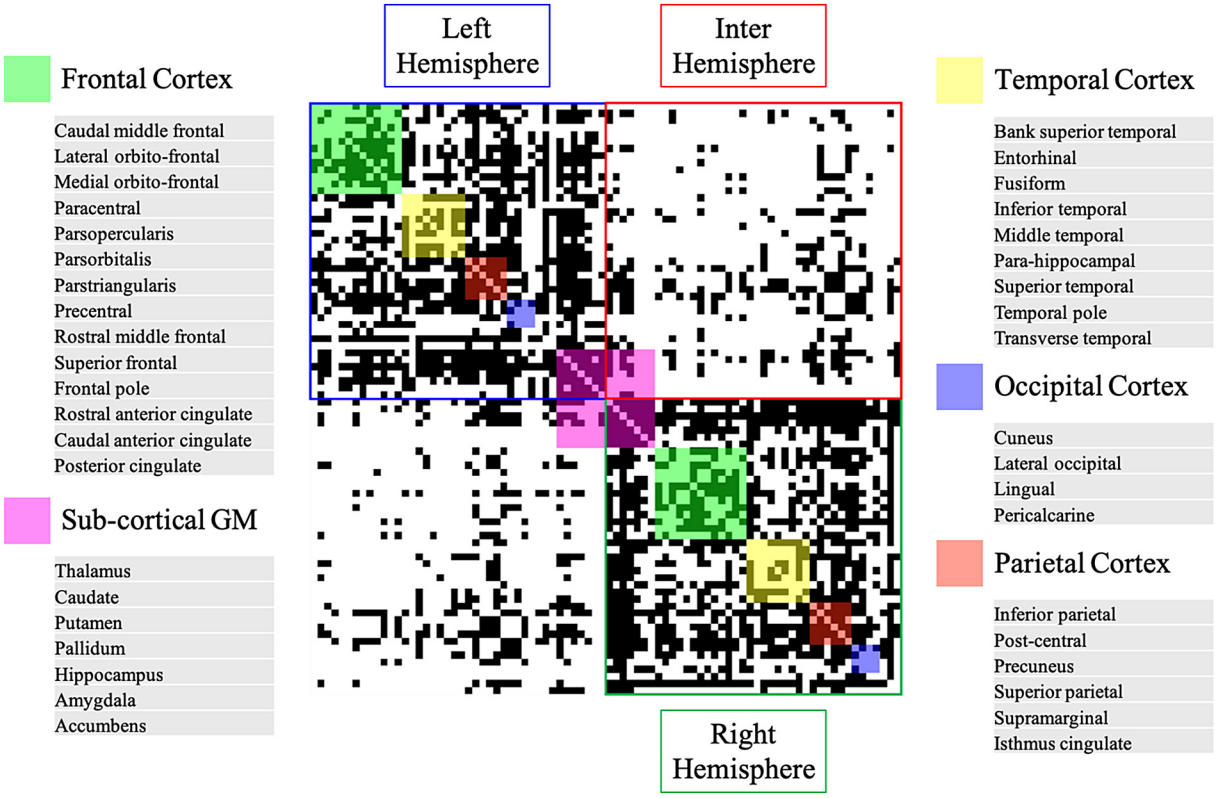

Fig. 2. Schematic representation of the connectivity matrix subdivision in different networks, including left-, right-, and inter- hemispheres networks and lobes networks. The cortical regions in each lobe are also reported.

analyzed using the following three metrics: the transitivity (***T***) which is the ratio between the number of triangles and the number of triplets in the graph, the assortativity (***r***) which is the Pearson coefficient between the degrees of two nodes at the extremities of an edge, and the modularity (***Q***) which is the difference between the number of intra-modules connections and the number of inter-modules connections. Four nodal graph metrics were also computed. The degree (k_i) represents the number of connections of each node. The clustering coefficient (C_i) defined as the ratio between the number of triangles and the number of triplets around each node, measures the network's tendency to form dense local clusters. The betweenness centrality (B_i), defined as the ratio of the number of the shortest paths comprising the node to the total number of shortest paths in the graph, measures the hub property of the node. The nodal efficiency (E_i) defined as the mean of the inverse of the distance vector, measures the signal transmission efficiency.

Small-world properties of each subject's graph were estimated. First, a random graph with preserved degree distribution was generated. Then the characteristic path length (***L***) and the mean clustering coefficient (***C***) were estimated for both the subject and the random graph. Finally, **λ,** γ, and ***σ*** were estimated as follows:

$$\lambda = \frac{L_{subject}}{L_{random}}; \quad \gamma = \frac{C_{subject}}{C_{random}}; \quad \sigma = \frac{\gamma}{\lambda}$$

Compared with a random network, small-world networks are known to have similar ***L*** and higher ***C***, resulting in $\lambda \approx 1$, $\gamma > 1$, and $\sigma > 1$.(Shuman et al., 2013)

All the metrics, except graph density, were computed based on the binarized connectivity matrices using the brain connectivity toolbox on Matlab.(Shaw et al., 2006)

2.6. Statistical analysis

As previously described in Karama et al.(Simpson et al., 2013), a factor analysis was performed on the correlation matrix of the ten WISC subtests in order to explore their inter-correlations and to extract intelligence domains not biased by the factor "g". First, a factor analysis using the oblique "promax" rotation was applied to the subtests, defining the principal intelligence domains. Second, an unrotated factor analysis was performed to extract the g-score, defined as the scores of the first factor component. Finally, the correlations between each intelligence domains and the g-score were processed to extract their residuals, considered as g-unbiased intelligence domains.

As previously described by Privado et al.(Song et al., 2008), a principal component analysis (PCA) was performed to explore potential groups of inter-correlated WM fiber-bundles, based on their diffusivity metrics (FA, AD, RD, MD). The resulting components were rotated to the simple structure using a "promax" rotation.

Partial correlations between g-unbiased intelligence domains and graph network metrics or diffusivity components were calculated in the total subject sample. A general linear model (GLM) was used to investigate the relationship between each intelligence domain and the diffusion metrics of the WM fiber-bundles, as well as the global and nodal graph metrics. Age and sex were added to the linear model as cofactors in order to account for any imbalance effect. The general expression of this model was as follows:

Intelligence domain~(*diffusion*/*graph*) *metric* + *Age* + *Gender*

Significance of all predictors for each fit was tested by applying analysis-of-variance and analysis-of-deviance with a 5% significance level. All statistical analysis were computed using R and the "psych" library.(Sowell et al., 2003) In order to correct for multiple comparisons between the local graph metrics, Sidak correction was applied to the *p*-values.

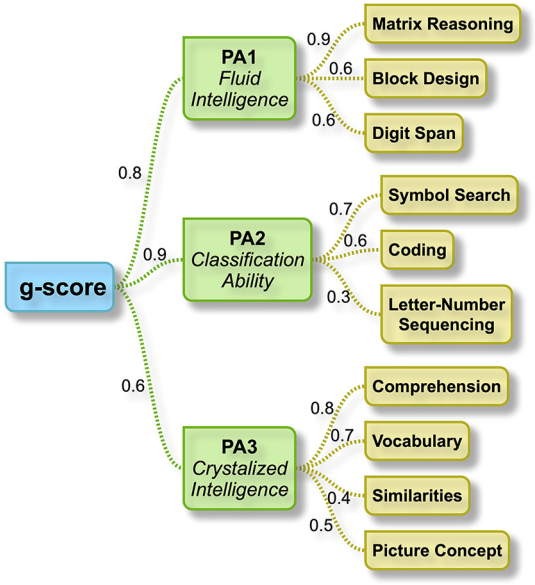

Fig. 3. The g-score, obtained using a factor analysis of the ten WISC subtests, was composed of three major broad domains, named "fluid intelligence" (PA1), "classification ability" (PA2), and "crystalized intelligence" (PA3).

3. Results

3.1. Intelligence factor analysis

Based on the ten WISC-IV subtests data, three broad g-score domains were defined by the factor analysis as shown in Fig. 3. Table 1 shows the descriptive statistics for the ten intelligence measures and the correlations among them. The first domain (PA1) including the matrix reasoning, block design, digit span, and similarities subtests, is named "fluid intelligence". The second domain (PA2) including the symbol search, coding, and letter-number sequencing subtests, is named "Classification ability"; and the third domain including the comprehension, vocabulary, and picture concept subtests, is named "crystalized intelligence". A second factor analysis, based on the three major intelligence domains, was then applied on the correlation matrix to define the g-score and the g-unbiased intelligence domains (PA1-g, PA2-g, and PA3-g; Table S2 in the supplementary data).

3.2. Fiber-bundles analysis

Based on the diffusion data of the seventeen WM fiber-bundles, broad components of fiber-bundles were defined by a factor analysis. First performed on FA values of the WM fiber-bundles (Table S2 in supplementary materials), the factor analysis extracted five broad components with eigenvalues of 6.93, 1.78, 1.40, 1.30, and 1.17, explaining 74% of the total variance (41%, 10%, 8%, 8%, and 7%). The first component (FA-Comp1) showed high loadings for the Fmajor, Fminor, left and right ILF and left hippocampal part of the Cing and left IFOF. The second component (FA-Comp2) comprised the left and right Unc, the right hippocampal part of the Cing and the right IFOF, whereas the third component (FA-Comp3) showed high loadings for the left and right cingular parts of the Cing and the right SLF. The fourth component (FA-Comp4) comprised the left and right CST, whereas the fifth component (FA-Comp5) showed high loadings for the fornix and the left SLF.

When performed on AD values of the WM fiber bundles (Table S3 in supplementary data), four broad components were obtained with eigenvalues of 7.22, 2.60, 1.56, and 1.12, explaining 74% of the total variance (42%, 15%, 9%, and 7%). The first component (AD-Comp1) showed high loadings for the Fmajor and Fminor, and for the right hippocampal part of the Cing, CST, IFOF, ILF, SLF, and Unc. The second component (AD-Comp2) comprised the left IFOF, ILF, SLF, and Unc. The third component (AD-Comp3) showed high loadings for the fornix and the left and right cingular part of the Cing. Finally, the fourth (AD-Comp4) component comprised the left hippocampal part of the Cing and CST.

As reported in Table 2, the broad components based on AD and FA values of the WM fiber bundles were further correlated to the intelligence domains. First, significant positive correlations were observed between AD-Comp1 and PA1, PA2, PA3, and g-score. Also, significant positive correlations were observed between AD-Comp2 and PA1, g-score and PA1-g, and between AD-Comp4 and PA3-g. Finally, a significant negative correlation was observed between AD-Comp2 and PA2-g. Second, significant positive correlations were observed between FA-Comp1 and PA1 and between FA-Comp5 and PA2 and g-score. A significant negative correlation between FA-Comp1 and PA2-g was observed. The factor analysis was also performed on the radial and mean diffusivities of WM fiber-bundles and showed no significant correlations with intelligence (Loadings matrices are reported in Tables S4 and S5 of supplementary data).

3.3. Graph analysis

Structural brain networks were successfully reconstructed using a threshold of 0.25 and 1'000'000 fibers. The resulting networks showed overall small world characteristics for all subjects with a mean σ of 1.62, a mean γ of 1.74, and a mean λ of 1.08.

Table 1
Correlation matrix and descriptive statistics of the ten WISC-IV subtests (1: Block Design, 2: Similarities, 3: Digit span, 4: Picture concept, 5: Coding, 6: Vocabulary, 7: Letter-Number, 8: Matrix reasoning, 9: Comprehension, 10: Symbol search).

	1	2	3	4	5	6	7	8	9	10
1		0.42**	0.43**	0.19	0.17	0.27	0.42**	0.56***	0.23	0.20
2			0.57***	0.52***	0.12	0.43**	0.51***	0.46**	0.41**	0.33*
3				0.43**	0.19	0.30	0.54***	0.49***	0.44**	0.03
4					0.32*	0.30	0.52***	0.21	0.34*	0.16
5						0.30	0.42**	0.21	0.09	0.41**
6							0.43**	0.13	0.56***	0.19
7								0.53***	0.35*	0.36*
8									0.23	0.30
9										−0.06
10										
Mean	13.19	15.86	12.28	12.6	10.86	15.93	11.44	13.37	14.47	11.14
sd	3.86	3.11	3.13	3.25	3.19	3.06	3.11	3.02	3.38	2.62

* $p < 0.05$.
** $p < 0.01$.
*** $p < 0.001$.

Table 2
Correlations between WM fiber-bundles diffusivity components of fractional anisotropy (FA) and axial diffusivity (AD), and intelligence domains (PA1, PA2, and PA3), g-score, and g-unbiased intelligence domains (PA1-g, PA2-g, and PA3-g).

		PA1	PA2	PA3	g-score	PA1-g	PA2-g	PA3-g
AD	Comp-1	0.397**	0.402**	0.259*	0.433**			
	Comp-2	0.496**			0.353*	0.197*	−0.116*	
	Comp-4							0.257**, ***
FA	Comp-1	0.323*					−0.112*	
	Comp-5		0.320*		0.327*			

* $p < 0.05$.
** $p < 0.01$.
*** $p < 0.05$ for effect of age.

Table 3
Correlation slopes between global graph metrics, namely the density (***D***), assortativity (***r***), transitivity (***T***), modularity (***Q***), characteristic path length (***L***), and efficiency (***E***) in different brain networks (whole brain, inter-hemispheres, left and right hemispheres, lobes, and subcortical nuclei) and intelligence domains (PA1, PA2, PA3, g-score, and g-unbiased PA1-g, PA2-g, PA3-g).

		g-score	PA1	PA2	PA3	PA1-g	PA2-g	PA3-g
Whole brain	*D*	16.87**	19.06***	15.24*	–	–	–	–
Inter-hemisphere	*D*	9.20*	11.58**	–	–	–	–	–
	E	–	–	–	–	4.82*	–	–
	L	–	–	–	–	0.30*	–	–
	Q	–	–	–	–	1.68*	–	–
	T	–	–	–	–	–	−3.25*	–
Left Hemisphere	*D*	19.52**	19.48**	19.53*	–	–	–	–
	Q	–	–	–	–	–	–	−16.59*
Right Hemisphere	*D*	13.17*	12.76*	12.68*	–	–	–	–
	T	–	–	–	–	−20.26*	–	–
Frontal	*Q*	–	–	–	–	–	–	11.46*
	T	−14.26*	–	−14.37*	–	–	–	–
Parietal	*D*	18.24***	20.16***	15.86***	–	–	–	–
	Q	–	−10.85**	–	–	−4.87*	–	–
	r	−7.27**	−8.12**	−6.24*	–	–	–	–
Temporal	*E*	−45.01*	−52.19*	–	–	–	–	–
	L	10.22*	12.12**	–	–	–	–	–
	Q	−225.66*	–	−218.25*	–	–	–	–
	r	6.13**	5.82*	5.81*	–	–	–	–
Occipital	*D*	–	2.67*	–	–	–	–	–
	E	–	–	–	–	–	–	18.84**
	L	–	–	–	–	–	–	−5.38**
	T	–	–	–	–	–	–	2.68*, #
Subcortical	*E*	–	–	–	4.43*	–	–	–
	L	–	–	–	–	–	–	−1.13**
	r	–	–	–	2.86*	–	–	2.01*

* $p < 0.05$.
** $p < 0.01$.
*** $p < 0.001$.
# $p < 0.05$ for the effect of age.

3.4. Global graph metrics

Correlations between graph metrics and the three intelligence domains, the g-score, and the g-unbiased intelligence domains are reported in Table 3. PA1, PA2, and g-score showed significant correlations with the density in the whole brain (Fig. 4). In the inter-hemispheric network, PA1 and g-score were positively correlated with density, PA1-g was positively correlated with efficiency, characteristic

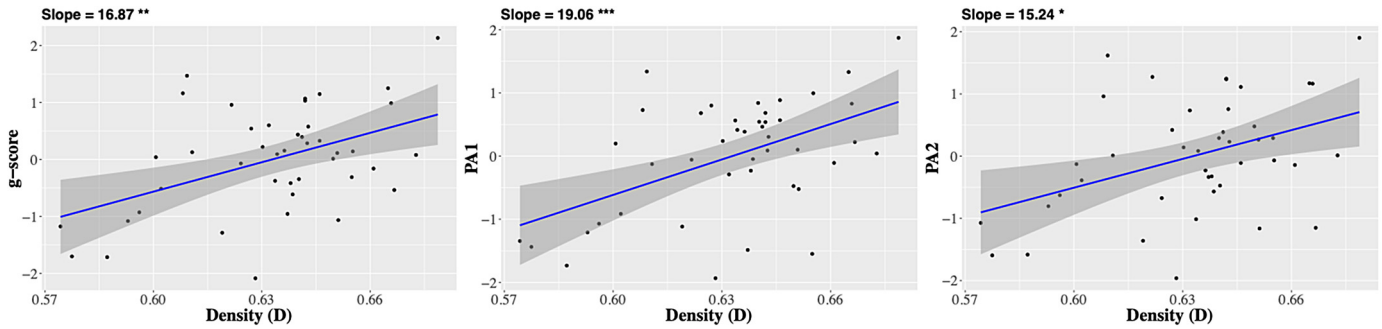

Fig. 4. Significant positive correlations measured between graph density in the whole brain network and the g-score ($p < 0.01$), the fluid intelligence domain (PA1; $p < 0.001$), and the classification ability domain (PA2; $p < 0.05$).

path length, and modularity, and PA2-g was negatively correlated with transitivity. PA1, PA2, and g-score were positively correlated with density in both left and right hemispheres, whereas PA1-g showed negative correlations with transitivity in the right hemisphere and PA3-g with modularity in the left hemisphere.

Global graph metrics were also measured in brain networks of lobes, namely the frontal, parietal, occipital, and temporal lobes, as well as in the sub-cortical nuclei. In the frontal lobe, PA3-g was positively correlated with modularity, whereas PA2 and g-score were negatively correlated with transitivity. In the parietal lobe, PA1, PA2, and g-score were positively correlated with density, while PA1 and PA1-g were negatively correlated with modularity. Also, PA1, PA2, and g-score were negatively correlated with assortativity. In the occipital lobe, PA1 was positively correlated with density. PA3-g was positively correlated with efficiency and transitivity, but negatively correlated with characteristic path length. In the temporal lobe, PA1 and g-score were positively correlated with characteristic path length and assortativity and negatively with efficiency. PA2 was positively correlated with assortativity and negatively with modularity. Also, g-score was negatively correlated with modularity. Finally, in the sub-cortical network, PA3 was positively correlated with efficiency and assortativity, while PA3-g was negatively correlated with characteristic path length and positively correlated with assortativity.

3.5. Nodal graph metrics

Significant correlations were observed between intelligence domains and g-score and local graph metrics in all the brain lobes. However, after correcting p-values for multiple comparisons (84 graph nodes), only few correlations remained significant. More in details, PA1-g was positively correlated with the degree and betweenness centrality, and negatively with clustering coefficient and local efficiency in the right precuneus node (Fig. 5). Also, PA1-g was negatively correlated with the degree in the right isthmus cingulate node.

4. Discussion

In this work, WM structural connectivity was measured using fiber-bundle analysis as well as graph theory method. To our knowledge, this study is the first to correlate children intelligence with both global and local graph metrics of brain networks.

The main finding of this study was the observation of numerous significant correlations between different global graph metrics and intelligence domains. First, the increase of density with the general intelligence domains (g-score, PA1, and PA2) in the whole brain, the left and right hemispheres, and the inter-hemisphere networks demonstrated that a high level of intelligence is associated with increased WM connectivity. More specifically, the graph density in whole brain and hemisphere networks was correlated with PA1 and PA2 but not with PA3 intelligence domains, showing the predominance of fluid intelligence and classification abilities. Second, the decreased segregation properties (modularity and transitivity) with the general intelligence domains (g-score, PA1, and PA2) in the frontal (PA2), parietal (PA1), and temporal (g-score and PA2) lobes networks showed that the main intelligence domains are related to homogenous brain organization. These correlations observed between frontal and temporo-parietal regions and intelligence are in agreement with the meta-analysis of Jung and Haier,(Gogtay et al., 2004) and Basten et al.(Gray et al., 2003) Nevertheless, as concluded by Basten et al.,(Gray et al., 2003) one should carefully distinguish structural and functional brain correlates of intelligence. These correlations confirmed the important role of parietal and temporal functions, in intelligence processes, including visuo-spatial and classification abilities, unconsciousness, memory (mirror neurons) and emotion.(Spearman, 1904; Squire and Zola-Morgan, 1991) In contrast, the third broad intelligence domain, named crystalized intelligence (PA3 and PA3-g), was mainly associated to increased integration properties in the occipital lobe and sub-cortical nuclei networks. This finding is in agreement with the previous report of Colom et al., showing that crystalized intelligence correlates mainly with occipital regions.(Tamnes et al., 2010) These findings on global network organization support the model proposed by Barbey,(Haier et al., 2004) in which high intelligence is related to a balance between high integration (high density) and mean segregation (modularity and transitivity) levels in the network, which correspond to the definition of a small-world network as observed in this study.

To further explore the relationship between intelligence and brain

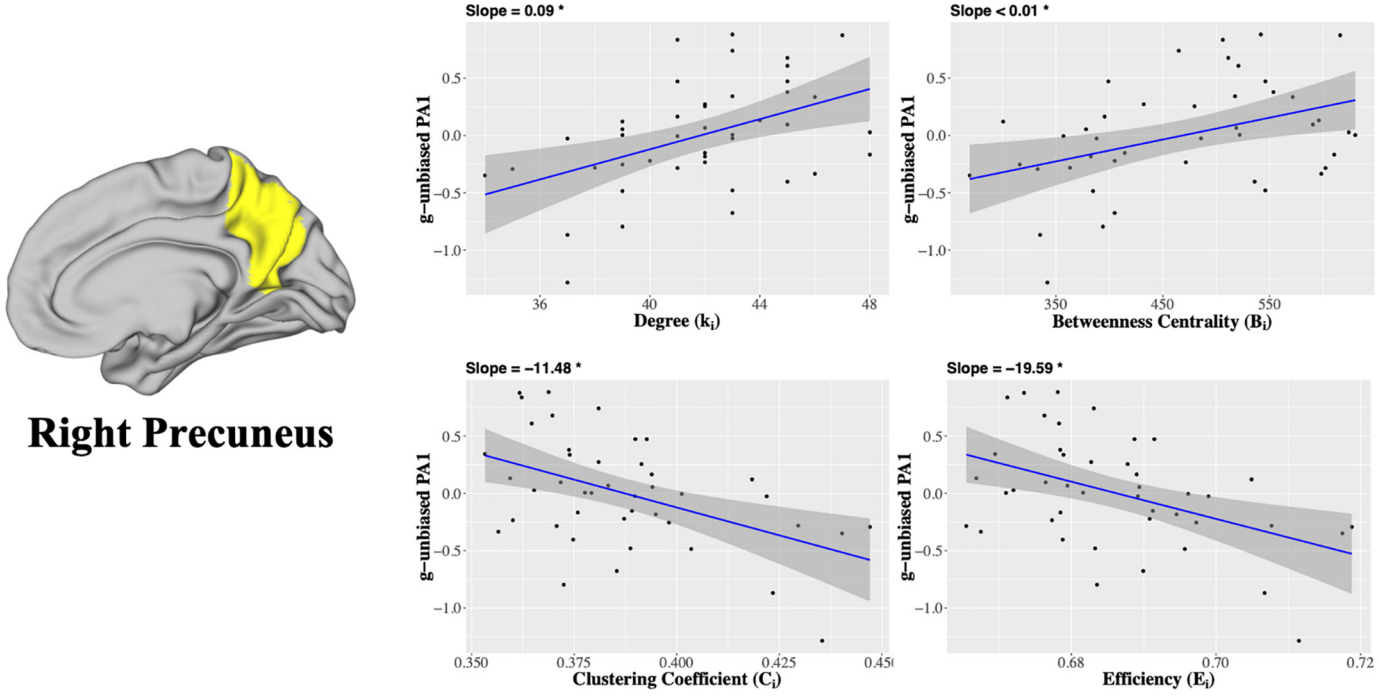

Fig. 5. Correlations between PA1-g intelligence domain and local graph metrics in the right precuneus node.

organization at a lower scale, local graph metrics were computed. Associations were mainly found in the parietal, temporal, and frontal lobes, which correspond to the P-FIT regions.(Gogtay et al., 2004) However, after multi-comparison correction, only correlations in the parietal lobe remained significant. The four metrics, measured in the right precuneus, showed a better network integration in relation with the g-unbiased fluid intelligence (PA1-g). This result is in agreement with previous studies, highlighting the importance of the precuneus in visuo-spatial abilities and self-conciousness.(Team, 2015; Tournier et al., 2012)

These results on structural brain network organization were confirmed by the diffusivity measurements obtained from the major WM fiber-bundles. Indeed, positive correlations were observed between AD values and intelligence domains. Based on the hypothesis that AD values reflect myelination and axonal density or diameter,(Uehara et al., 2014; Varentsova et al., 2014) these findings confirmed the relationship between WM fiber-tracts integrity and intelligence and suggest the potential interest of AD as a marker of general intelligence. More specifically, the correlation with g-score and g-intelligence domains (PA1, PA2, and PA3) were mainly located in the right fiber-bundles (AD-Comp1), while the correlations with g-unbiased intelligence domains were mainly located in the left fiber-bundles (AD-Comp2). These results may suggest a potential lateralization of the intelligence axonal substrate, with the general intelligence being more weighted by the right WM fiber-bundles, and the g-unbiased intelligence being more weighted by the left WM fiber-bundles.

5. Methodological limitations

From a methodological perspective, this study may suffer from few limitations. First, the diffusion acquisition was limited to 24 directions, which is relatively low compared to current research standards in diffusion imaging. Nonetheless, potential crossing-fibers errors were minimized by using spherical deconvolution instead of classical diffusion tensor model. Second, this study recruited a relatively low number of participants, which is mostly related to the targeted population of young children. Third, the unbalanced ratio of girls and boys was overcome by including the gender effect in the statistical analysis. This limitation is often encountered in high potential children studies, as girls present the ability to “over-adapt” which leads to an under-diagnosis of high IQ girls. Finally, our subjects' age was limited to the range of eight to twelve years old. At this age, the maturation of prefrontal cortex is not complete, which may explain the lack of finding in this region.(Wechsler, 2004; Wickett et al., 2000)

6. Conclusion

Our findings showed that both inter- and intra-hemispheric WM integrity are enhanced in children with high intellectual abilities. In agreement with the literature, these results confirmed that diffusion metrics measured in WM fiber-bundles constitute accurate and quantitative markers of intelligence. Furthermore, high intelligence neural substrate is related to a high fiber density, optimally distributed through integrated and homogeneous networks. This study confirmed the sensitivity and the accuracy of such graph-based methods for the investigation of brain topological organization.

Declaration of interest statement

We wish to confirm that there are no known conflicts of interest associated with this publication. This work was financed by APICIL Foundation and SHIRE International which had no role in study design, data collection and analysis, decision to publish, or preparation of the manuscript.

We confirm that the manuscript has been read and approved by all named authors and that there are no other persons who satisfied the criteria for authorship but are not listed. We further confirm that the order of authors listed in the manuscript has been approved by all of us.

We confirm that we have given due consideration to the protection of intellectual property associated with this work and that there are no impediments to publication, including the timing of publication, with respect to intellectual property. In so doing we confirm that we have followed the regulations of our institutions concerning intellectual property.

We further confirm that any aspect of the work covered in this manuscript has been conducted with the ethical approval of all relevant bodies and that such approvals are acknowledged within the manuscript.

We understand that the Corresponding Author is the sole contact for the Editorial process (including Editorial Manager and direct communications with the office). He is responsible for communicating with the other authors about progress, submissions of revisions and final approval of proofs.

Signed by all authors as follows

Gabriel Kocevar, Ilaria Suprano, Claudio Stamile, Salem Hannoun, Pierre Fourneret, Olivier Revol, Fanny Nusbaum, and Dominique Sappey-Marinier.

Acknowledgement

Gabriel Kocevar and Ilaria Suprano were funded by a national grant from the French government. Claudio Stamile was funded by an EU-funded FP7-PEOPLE-2012-ITN project 316679 TRANSACT. This work was made possible by APICIL Foundation and SHIRE International financial supports. The funders had no role in study design, data collection and analysis, decision to publish, or preparation of the manuscript. Authors would like to thank the staff of the CERMEP-Imagerie du Vivant for their help with MRI data acquisition.

Appendix A. Supplementary data

Supplementary data to this article can be found online at https://doi.org/10.1016/j.intell.2018.12.003.

References

Barbey, A. K. (2018). Network Neuroscience Theory of Human Intelligence. *Trends in Cognitive Sciences, 22*(1), 8–20. https://doi.org/10.1016/j.tics.2017.10.001.

Basser, P. J., Mattiello, J., & Lebihan, D. (1994). Estimation of the Effective Self-Diffusion Tensor from the NMR Spin Echo. *Journal of Magnetic Resonance - Series B, 103*(3), 247–254. https://doi.org/10.1006/jmrb.1994.1037.

Basser, P. J., Basser, P. J., Jones, D. K., & Jones, D. K. (2002). Diffusion-tensor MRI: Theory, experimental design and data analysis - a technical review. *NMR in Biomedicine, 15*, 456–467. https://doi.org/10.1002/nbm.783.

Basten, U., Hilger, K., & Fiebach, C. J. (2015). Where smart brains are different: A quantitative meta-analysis of functional and structural brain imaging studies on intelligence. *Intelligence, 51*(May), 10–27. https://doi.org/10.1016/j.intell.2015.04.009.

Beaulieu, C. (2002). The basis of anisotropic water diffusion in the nervous system - a technical review. *NMR in Biomedicine, 15*(7–8), 435–455. https://doi.org/10.1002/nbm.782.

Binet, A. (1905). The development of intelligence in children. *L'Année Psychol, 12*, 191–244.

Bullmore, E. T., & Sporns, O. (2009). Complex brain networks: Graph theoretical analysis of structural and functional systems. *Nature Reviews. Neuroscience, 10*(3), 186–198. https://doi.org/10.1038/nrn2575.

Carroll, J. B. (1993). *Human Cognitive Abilities: A survey of Factor-Analytic Studies.* New York: Cambridge University Presshttps://doi.org/10.1017/CBO9780511571312.

Clayden, J. D., Jentschke, S., Muñoz, M., et al. (2012). Normative development of white matter tracts: Similarities and differences in relation to age, gender, and intelligence. *Cerebral Cortex, 22*(8), 1738–1747. https://doi.org/10.1093/cercor/bhr243.

Colom, R., Haier, R. J. J., Head, K., et al. (2009). Gray matter correlates of fluid, crystallized, and spatial intelligence: Testing the P-FIT model. *Intelligence, 37*(2), 124–135. https://doi.org/10.1016/j.intell.2008.07.007.

Colom, R., Karama, S., Jung, R. E., & Haier, R. J. (2010). Human intelligence and brain networks. *Dialogues in Clinical Neuroscience, 12*(4), 489–501.

Desco, M., Navas-Sanchez, F. J., Sanchez-González, J., et al. (2011). Mathematically gifted adolescents use more extensive and more bilateral areas of the fronto-parietal network than controls during executive functioning and fluid reasoning tasks.

NeuroImage, 57(1), 281–292. https://doi.org/10.1016/j.neuroimage.2011.03.063.
Desikan, R. S., Ségonne, F., Fischl, B., et al. (2006). An automated labeling system for subdividing the human cerebral cortex on MRI scans into gyral based regions of interest. *NeuroImage, 31*(3), 968–980. https://doi.org/10.1016/j.neuroimage.2006.01.021.
Duncan, J. (2000). A Neural Basis for General Intelligence. *Science (80-). 289*(5478), 457–460. https://doi.org/10.1126/science.289.5478.457.
Dunst, B., Benedek, M., Koschutnig, K., Jauk, E., & Neubauer, A. C. (2014). Sex differences in the IQ-white matter microstructure relationship: A DTI study. *Brain and Cognition, 91*, 71–78. https://doi.org/10.1016/j.bandc.2014.08.006.
Gogtay, N., Giedd, J. N., Lusk, L., et al. (2004). Dynamic mapping of human cortical development during childhood through early adulthood. *Proceedings of the National Academy of Sciences of the United States of America, 101*(21), 8174–8179. https://doi.org/10.1073/pnas.0402680101.
Gray, J. R., Chabris, C. F., & Braver, T. S. (2003). Neural mechanisms of general fluid intelligence. *Nature Neuroscience, 6*(3), 316–322. https://doi.org/10.1038/nn1014.
Hagmann, P., Kurant, M., Gigandet, X., et al. (2007). Mapping human whole-brain structural networks with diffusion MRI. *PLoS One, 2*(7), https://doi.org/10.1371/journal.pone.0000597.
Haier, R. J., Jung, R. E., Yeo, R. A., Head, K., & Alkire, M. T. (2004). Structural brain variation and general intelligence. *NeuroImage, 23*(1), 425–433. https://doi.org/10.1016/j.neuroimage.2004.04.025.
Harris, G., & Galton, F. (1870). Hereditary genius. *Journal des Anthropologues, 1*(1), 56. https://doi.org/10.2307/3024796.
Hilger, K., Ekman, M., Fiebach, C. J., & Basten, U. (2017). Intelligence is associated with the modular structure of intrinsic brain networks. *Scientific Reports*. https://doi.org/10.1038/s41598-017-15795-7.
Jenkinson, M., Beckmann, C. F., Behrens, T. E. J., Woolrich, M. W., & Smith, S. M. (2012). Fsl. *NeuroImage, 62*(2), 782–790. https://doi.org/10.1016/j.neuroimage.2011.09.015.
Jones, D. K., Knösche, T. R., & Turner, R. (2013). White matter integrity, fiber count, and other fallacies: The do's and don'ts of diffusion MRI. *NeuroImage, 73*, 239–254. https://doi.org/10.1016/j.neuroimage.2012.06.081.
Jung, R. E., & Haier, R. J. (2007). The Parieto-Frontal Integration Theory (P-FIT) of intelligence: Converging neuroimaging evidence. *The Behavioral and Brain Sciences, 30*(02), 135. https://doi.org/10.1017/S0140525X07001185.
Karama, S., Colom, R., Johnson, W., et al. (2011). Cortical thickness correlates of specific cognitive performance accounted for by the general factor of intelligence in healthy children aged 6 to 18. *NeuroImage, 55*(4), 1443–1453. https://doi.org/10.1016/j.neuroimage.2011.01.016.
Kim, D.-J. J., Davis, E. P., Sandman, C. A., et al. (2016). Children's intellectual ability is associated with structural network integrity. *NeuroImage, 124*, 550–556. https://doi.org/10.1016/j.neuroimage.2015.09.012.
Kocevar, G., Stamile, C., Hannoun, S., et al. (2016). Graph theory-based brain connectivity for automatic classification of multiple sclerosis clinical courses. *Frontiers in Neuroscience, 10*(October), 1–11. https://doi.org/10.3389/fnins.2016.00478.
Lee, K. H., Choi, Y. Y., Gray, J. R., et al. (2006). Neural correlates of superior intelligence: Stronger recruitment of posterior parietal cortex. *NeuroImage, 29*(2), 578–586. https://doi.org/10.1016/j.neuroimage.2005.07.036.
Li, Y., Liu, Y., Li, J., et al. (2009). Brain Anatomical Network and Intelligence. Sporns O, ed. *PLoS Comput Biol. 5*(5), e1000395. https://doi.org/10.1371/journal.pcbi.1000395.
Lou, H. C., Luber, B., Crupain, M., et al. (2004). Parietal cortex and representation of the mental self. *Proceedings of the National Academy of Sciences, 101*(17), 6827–6832. https://doi.org/10.1073/pnas.0400049101.
McDaniel, M. A. (2005). Big-brained people are smarter: A meta-analysis of the relationship between in vivo brain volume and intelligence. *Intelligence, 33*(4), 337–346. https://doi.org/10.1016/j.intell.2004.11.005.
Mori, S., & Zhang, J. (2006). Principles of Diffusion Tensor Imaging and its applications to Basic Neuroscience Research. *Neuron, 51*(5), 527–539. https://doi.org/10.1016/j.neuron.2006.08.012.
Muetzel, R. L., Mous, S. E., van der Ende, J., et al. (2015). White matter integrity and cognitive performance in school-age children: A population-based neuroimaging study. *NeuroImage, 119*, 119–128. https://doi.org/10.1016/j.neuroimage.2015.06.014.
Navaschez, F. J., Alemez, Y., Schez-Gonzalez, J., et al. (2014). White matter microstructure correlates of mathematical giftedness and intelligence quotient. *Human Brain Mapping, 35*(6), 2619–2631. https://doi.org/10.1002/hbm.22355.
Nusbaum, F., Hannoun, S., Kocevar, G., et al. (2017). Hemispheric differences in White Matter Microstructure between two Profiles of Children with High Intelligence Quotient vs. Controls: A Tract-based Spatial Statistics Study. *Frontiers in Neuroscience, 11*(APR), https://doi.org/10.3389/fnins.2017.00173.
Oshio, R., Tanaka, S., Sadato, N., Sokabe, M., Hanakawa, T., & Honda, M. (2010). Differential effect of double-pulse TMS applied to dorsal premotor cortex and precuneus during internal operation of visuospatial information. *NeuroImage, 49*(1), 1108–1115. https://doi.org/10.1016/j.neuroimage.2009.07.034.
Ourselin, S., Roche, A., Subsol, G., Pennec, X., & Ayache, N. (2001). Reconstructing a 3D structure from serial histological sections. *Image and Vision Computing, 19*(1–2), 25–31. https://doi.org/10.1016/S0262-8856(00)00052-4.
Privado, J., Román, F. J., Saénz-Urturi, C., Burgaleta, M., & Colom, R. (2017). Gray and white matter correlates of the big five personality traits. *Neuroscience, 349*, 174–184. https://doi.org/10.1016/j.neuroscience.2017.02.039.
Reuter, M., Schmansky, N. J., Rosas, H. D., & Fischl, B. (2012). Within-subject template estimation for unbiased longitudinal image analysis. *NeuroImage, 61*(4), 1402–1418. https://doi.org/10.1016/j.neuroimage.2012.02.084.
Rubinov, M., & Sporns, O. (2010). Complex network measures of brain connectivity: Uses and interpretations. *NeuroImage, 52*(3), 1059–1069. https://doi.org/10.1016/j.neuroimage.2009.10.003.
Schmithorst, V. J., Wilke, M., Dardzinski, B. J., & Holland, S. K. (2005). Cognitive functions correlate with white matter architecture in a normal pediatric population: A diffusion tensor MRI study. *Human Brain Mapping, 26*(2), 139–147. https://doi.org/10.1002/hbm.20149.
Shaw, P., Greenstein, D., Lerch, J., et al. (2006). Intellectual ability and cortical development in children and adolescents. *Nature, 440*(7084), 676–679. https://doi.org/10.1038/nature04513.
Shuman, D. I., Narang, S. K., Frossard, P., Ortega, A., & Vandergheynst, P. (2013). The emerging field of signal processing on graphs: Extending high-dimensional data analysis to networks and other irregular domains. *IEEE Signal Processing Magazine, 30*(3), 83–98. https://doi.org/10.1109/MSP.2012.2235192.
Simpson, S. L., Bowman, F. D., & Laurienti, P. J. (2013). Analyzing complex functional brain networks: Fusing statistics and network science to understand the brain. *Stat Surv. 7*, 1–36. https://doi.org/10.1214/13-SS103.
Song, M., Zhou, Y., Li, J., et al. (2008). Brain spontaneous functional connectivity and intelligence. *NeuroImage, 41*(3), 1168–1176. https://doi.org/10.1016/j.neuroimage.2008.02.036.
Sowell, E. R., Peterson, B. S., Thompson, P. M., Welcome, S. E., Henkenius, A. L., & Toga, A. W. (2003). Mapping cortical change across the human life span. *Nature Neuroscience, 6*(3), 309–315. https://doi.org/10.1038/nn1008.
Spearman, C. (1904). General Intelligence, Objectively Determined and measured. *The American Journal of Psychology, 15*(2), 201. https://doi.org/10.2307/1412107.
Squire, L. R., & Zola-Morgan, S. (1991). The Medial Temporal Lobe memory System. *Sci New Ser. 253*(5026), 1380–1386. https://doi.org/10.1126/science.1896849.
Tamnes, C. K., Østby, Y., Walhovd, K. B., Westlye, L. T., Due-Tønnessen, P., & Fjell, A. M. (2010). Intellectual abilities and white matter microstructure in development: A diffusion tensor imaging study. *Human Brain Mapping, 31*(10), 1609–1625. https://doi.org/10.1002/hbm.20962.
Team, R. D. C. (2015). R: A Language and Environment for Statistical Computing. *R Found Stat Comput. 1*, 409. https://doi.org/10.1007/978-3-540-74686-7.
Tournier, J.-D., Calamante, F., & Connelly, A. (2012). MRtrix: Diffusion tractography in crossing fiber regions. *International Journal of Imaging Systems and Technology, 22*(1), 53–66. https://doi.org/10.1002/ima.22005.
Uehara, T., Yamasaki, T., Okamoto, T., et al. (2014). Efficiency of a “Small-World” Brain Network Depends on Consciousness Level: A Resting-State fMRI Study. *Cerebral Cortex, 24*(6), 1529–1539. https://doi.org/10.1093/cercor/bht004.
Varentsova, A., Zhang, S., & Arfanakis, K. (2014). Development of a high angular resolution diffusion imaging human brain template. *NeuroImage, 91*, 177–186. https://doi.org/10.1016/j.neuroimage.2014.01.009.
Wechsler, D. (2004). *The Wechsler Intelligence Scale for Children—Fourth Edition*.
Wickett, J. C., Vernon, P. A., & Lee, D. H. (2000). Relationships between factors of intelligence and brain volume. *Pers Individ Dif. 29*(6), 1095–1122. https://doi.org/10.1016/S0191-8869(99)00258-5.